Hindawi
Shock and Vibration
Volume 2022, Article ID 3690915, 11 pages
https://doi.org/10.1155/2022/3690915

Research Article

Experimental Study on the Dynamic Mechanical Properties of a Jointed Rock Mass under Impact Loading

Feng Wang,[1,2] Mengxiang Wang,[1] Haibo Wang,[1] Hao Wang,[1] and Qi Zong[1]

[1]*School of Civil Engineering and Architecture, Anhui University of Science and Technology, Huainan 232001, Anhui, China*
[2]*Beijing Zhongkeli Explosive Technology Engineering Co., Ltd., Beijing 101318, China*

Correspondence should be addressed to Mengxiang Wang; mxwang@aust.edu.cn

Received 5 August 2022; Revised 8 November 2022; Accepted 9 November 2022; Published 22 November 2022

Academic Editor: Kang Shao-Bo

The propagation law of blast stress waves in jointed rock masses is closely related to the characteristics of the joint filling medium. The water content and thickness of the filling medium affect the propagation characteristics of the blast stress wave in the joint surface. Based on similarity theory, mortar-red clay-mortar composite specimens with different moisture contents (36%, 39%, 42%, and 45%) and medium thicknesses (3 mm, 6 mm, and 9 mm) were prepared with red clay as the filling medium. The dynamic uniaxial compression test of the specimen under different strain rates was carried out by using a variable cross-section split Hopkinson compression bar with a diameter of 50 mm. The effects of strain rate, moisture content, and medium thickness on the stress wave propagation characteristics, dynamic stress-strain curve, peak stress, crushing energy consumption density, and crushing characteristics of mortar-red clay-mortar composite specimens were analyzed. The results show that the blocking effect of joints on stress waves increases significantly with increasing filling medium thickness and water content. With increasing strain rate, the peak stress and energy of the composite specimen increase and there is an obvious strain rate effect. With the increase in the thickness and moisture content of the filling medium, the peak stress, dynamic elastic modulus, energy consumption density per unit volume, and crushing degree of the specimen gradually decrease and the nonlinear deformation is more obvious. There is a good linear relationship between the peak stress and the thickness and moisture content of the filling medium. The existence of joints greatly weakens the damage effect of stress waves on the specimens behind the joints, and with the increase in the thickness and water content of the filling medium, the degree of damage to the specimens behind the joint surface decreases under the same impact pressure and the weakening effect becomes increasingly significant.

1. Introduction

As the product of long-term complex geological processes in nature, the internal structure of a rock mass is complex and there are numerous weak structural planes, such as joints, fissures, and faults. As one of the most representative structural planes in rock masses, joints often contain filling materials such as soft mud, sand, and rock debris, that is, filling joints. Their low strength and large deformation characteristics will change the mechanical properties of structural planes and even the whole rock mass and increase the instability of engineering rock masses [1–9]. During the drilling and blasting construction of a rock mass, when the explosion stress wave acts on the joint surface, the stress wave will be reflected and transmitted, resulting in the reduction of wave strength and the sharp attenuation of stress wave energy, which seriously hinders the propagation of waves. At the same time, the joints lead to the premature escape of explosion energy and explosion gas, overexcavation and underexcavation of rock contours, excessively large blasting rubble, and poor blasting effect, which seriously affect the efficiency and safety of the project [10–20]. Therefore, studying the stress wave propagation law of jointed rock masses under dynamic loads is of great significance to evaluate the stability of engineering rock masses and the safety of tunnel, slope, and underground engineering construction under blasting loads.

At present, scholars at home and abroad have carried out extensive research on the mechanical properties of jointed rock masses under dynamic loads using numerical simulations, model tests, and other methods. Dong et al. [21] studied the mesoscopic failure mode of a nonpenetrating jointed rock mass under impact loading, and the results showed that the longer the joint length was, the smaller the compressive strength of the specimen. Deng et al. [22] used the split Hopkinson pressure bar (SHPB) test device to analyze the mechanical properties of jointed rock masses from different aspects, such as geometric characteristics, aspect ratio effect, and strain rate. The research results are of great significance for understanding the dynamic mechanical properties of engineering rock masses and improving engineering blasting quality. Ma et al. [23] studied the dynamic mechanical properties of sandstone in deep roadways with different joint inclination angles. The results showed that the dynamic compressive strength and peak strain of the specimens first decreased and then increased with increasing joint inclination angle. Tsubota et al. [24] took gneiss as the research object, carried out dynamic tests on natural rock joints, revealed the mechanical properties of natural joints for the first time, and concluded that the surface conditions of rock joints, such as roughness, hardness, and degree of weathering, have a significant impact on the shear resistance of rocks. Niktabar et al. [25] conducted shear tests on joint specimens with different rough undulation angles and found that the shear strength of the specimens is in direct proportion to the rough undulation angle. Walton et al. [26] studied the influence of preset joints on main rock mass parameters such as stiffness, peak strength, and residual strength. Zhu et al. [27–30] systematically discussed the effects of joint mechanical parameters and incident wave parameters on stress wave propagation and the energy dissipation ratio in a jointed rock mass from two aspects of test and theoretical analysis. Li et al. [31] theoretically studied the propagation characteristics of stress waves in jointed rock masses filled with viscoelastic deformation characteristics by using the improved time domain recursive method. The variation trend of the transmission coefficient and reflection coefficient of the jointed rock mass with incident angle is considered the same. Research on the dynamics of filled jointed rock masses focuses mainly on the influence of filled joints on the propagation, attenuation, crack propagation mode, and energy propagation law of stress waves. Lei et al. [32] conducted an experimental study on the shear strength damage characteristics of jointed rock masses under freeze-thaw cycles. The results show that the damage variables of cohesion and friction angle of jointed rock increase nonlinearly with the increase in the number of freeze-thaw cycles. Therefore, the evolution model of joint shear damage under freeze-thaw cycles is established. Lin et al. [33] studied the distribution of the frost heaving stress of a water-bearing jointed rock mass under freeze-thaw cycles. The results show that the frost heaving stress of the specimens decreases significantly with the increase in the number of freeze-thaw cycles and water migration loss and increases with the increase in the mechanical strength and joint geometric size of the rocks and ice. In terms of numerical simulation, Bian [34] used ANSYS/LS-DYNA software to study the propagation and attenuation of stress waves corresponding to joints and the influence of joint geometry and fillings on its isolation effect. Liu et al. [35], Zhao et al. [36], and Yang et al. [37] used the universal discrete element code (UDEC) to simulate the propagation characteristics of stress waves in jointed rock masses. However, the influence of the thickness and water content of the joint filling body on the stress wave propagation law is rarely discussed.

This study is based on the cutting slope blasting project of the Panxian-Xingyi Expressway in Guizhou Province. The construction site is a karst medium low mountain landform. The subgrade is situated in the middle and upper parts of the slope, with steep and gentle slopes. The bedrock in the middle and upper parts of the slope is the limestone of the Yongningzhen Formation in the Lower Triassic system. Horizontal bedded joints have been developed; each layer is 0.3~0.5 m thick, and vertical joints have also been developed and filled with mud. During blasting excavation, the rock will bear a dynamic load. Based on the principle of similarity theory, the red clay in the engineering site was used as the filling medium to prepare mortar-red clay-mortar composite specimens with different moisture contents and thicknesses. Uniaxial impact compression tests were carried out on the specimens using a variable cross-section split Hopkinson pressure bar device with a diameter of 50 mm. The characteristics of stress wave propagation, dynamic stress-strain curve, dynamic compressive strength, energy dissipation, the change law of specimen breakage, and fracture characteristics of mortar-red clay-mortar composite specimens with different media moisture contents and thicknesses under impact load have been obtained. This study provides an experimental basis for engineering practice.

2. Test Plan

2.1. Sample Preparation. Due to the difficulty of on-site raw rock sampling, by drawing lessons from the research of domestic and foreign researchers in the field of rock simulation and taking advantage of the characteristics of easy preparation, easy availability of raw materials, and low cost of cement mortar, cement mortar was selected as the simulation material of jointed rock mass. In the test, the cement is P·O 32.5 ordinary Portland cement produced in Bagongshan, Huainan. The fine aggregate is natural river sand with a fineness modulus of 2.8, the water is natural tap water, and the mix proportion of the test piece is cement : medium sand : water = 2 : 2 : 1. After pouring, the test block was placed in the curing chamber with a curing humidity ≥95% and a temperature maintained at 20 ± 2°C for standard curing for 28 d. After coring, cutting, and grinding, the test piece was made into a cylindrical standard specimen with a diameter of 50 mm and height of 25 mm. The 28 d uniaxial compressive strength is 37 MPa, which meets the test requirements. To reduce the influence of the discrete type of specimen on the test results, it is necessary to measure the longitudinal wave velocity of the processed mortar specimen and select the mortar specimen with a similar longitudinal

wave velocity for the test [38]. At the same time, to distinguish the failure mode of the mortar specimens on both sides of the joint during the impact test, the mortar specimens close to the transmission rod are sprayed with red paint.

Red clay samples with water content of 36%, 39%, 42%, and 45% were prepared according to the test requirements. The required mass of soil and water was obtained through calculation, and then, the soil samples cooled to room temperature were successively added with water of corresponding quality through the steps of grinding, 2 mm screening, and drying. At the same time, the soil was fully stirred with a soil-mixing knife to evenly mix the red clay and water, and then, the mouth of the soil container was sealed with a fresh-keeping film. At the same time, the fresh-keeping film was covered with a wet towel and held for 24 hours so that the water could fully penetrate into the red clay. The red clay was made as shown in Figure 1.

2.2. The Test Process. The orthogonal test method was used, and the test variables were the thickness of the filling medium (d), moisture content of the filling medium (W), and strain rate. The range of thicknesses of the filling medium was 3 mm, 6 mm, and 9 mm, and the range of the water content of the filling medium was 36%, 39%, 42%, and 45%, respectively. Different impact pressures were selected to obtain different strain rates. At the same time, the impact pressure had an effect on the fracture morphology of the specimen. If the air pressure is small, the specimen cannot be destroyed in the impact test, so the influence law of the filling medium thickness and water content on the specimen fracture morphology cannot be compared. After test punching, four kinds of impact pressures (0.3, 0.4, 0.5, and 0.6 MPa) were finally selected to obtain different strain rates. According to the density, thickness and moisture content of the red clay, the required mass of the red clay is weighed in turn and then sandwiched between two mortar specimens to form the mortar-red clay-mortar composite specimen. To prevent water evaporation during the test, only one red clay sample with moisture content was configured during each impact test and the impact test was conducted immediately after the specimen was prepared. To ensure the accuracy of the test data and reduce the test error, three parallel test pieces were made for the same type of test, with a total of 144 mortar-red clay-mortar composite test pieces, and the test results were analyzed by selecting the group of test pieces closest to the average value. The structure of the specimen is shown in Figure 2.

2.3. SHPB Test Device. The impact compression test uses a 50 mm-diameter variable cross-section split Hopkinson compression bar test device system from the Impact Dynamics Laboratory of Anhui University of Technology. The impact rod, incident rod, and transmission rod are made of alloy steel, with a density of 7850 kg/m^3, an elastic modulus of 210 GPa, and a longitudinal wave velocity of 5190 m/s. The strain gauge at the incident rod adopts a BX120-3AA-type resistance strain gauge, the resistance value is $120 \pm 0.1\ \Omega$, and the sensitivity coefficient is $2.08 \pm 0.1\%$. Due to the small amplitude of the signal received by the transmission rod in the test, to make the data collected by the strain gauge meet the accuracy requirements, the HU-101B-120 semiconductor strain gauge was selected on the transmission rod, with a resistance value of $120 \pm 5\%\ \Omega$ and a sensitive coefficient of $110 \pm 5\%$ [39]. The structure of the test device is shown in Figure 3.

Four different impact pressures (0.3, 0.4, 0.5, and 0.6 MPa) were used for three different medium thicknesses (3 mm, 6 mm, and 9 mm), four different moisture content (36%, 39%, 42%, and 45%) composite specimens were subjected to shock compression tests, and the collected data were processed by the three-wave method [40, 41]. The relevant calculation formulas are as follows:

$$\begin{cases} \dot{\varepsilon}(t) = \dfrac{C_0}{l_s}\left[\varepsilon_i(t) - \varepsilon_r(t) - \varepsilon_t(t)\right], \\ \varepsilon(t) = \dfrac{C_0}{l}\displaystyle\int_0^t \left[\varepsilon_i(t) - \varepsilon_r(t) - \varepsilon_t(t)\right]\mathrm{d}t, \\ \sigma(t) = \dfrac{AE}{2A_S}\left[\varepsilon_i(t) + \varepsilon_r(t) + \varepsilon_t(t)\right], \end{cases}$$

$$\begin{cases} W_i(t) = AEC_0\displaystyle\int_0^t {\varepsilon_i}^2(t)dt, \\ W_r(t) = AEC_0\displaystyle\int_0^t {\varepsilon_r}^2(t)\mathrm{d}t, \\ W_t(t) = AEC_0\displaystyle\int_0^t {\varepsilon_t}^2(t)\mathrm{d}t, \end{cases} \tag{1}$$

$$W_s(t) = W_i(t) - W_r(t) - W_t(t),$$

$$\varepsilon_{\mathrm{d}} = \frac{W_s(t)}{V},$$

where $\varepsilon_i(t)$, $\varepsilon_r(t)$, and $\varepsilon_t(t)$ are the incident strain, reflected strain, and transmitted strain at time t, respectively, dimensionless; l_s is the thickness of the specimen, m; C_0, E are the compressional wave velocity and elastic modulus of the compression bar, m/s and MPa, respectively; A, A_S are the cross-sectional area of the pressure bar and the cross-sectional area of the specimen, m^2; W_i is the incident energy, W_r is the reflected energy, W_t is the transmitted energy, and W_t is the dissipated energy, J; ε_d is the crushing energy dissipation density, J/cm^3; V is the specimen volume, cm^3.

3. Results and Analysis

3.1. Effects of Strain Rate and Filling Medium on Stress Wave Propagation. Figure 4 shows the effective stress-time history curves of the mortar-red clay-mortar composite specimens with a filling medium moisture content W of 42% and a filling medium thickness d of 3 mm at different strain rates.

(a) (b)

Figure 1: Red clay specimen. (a) Dry red clay sample. (b) Sheng soil dish.

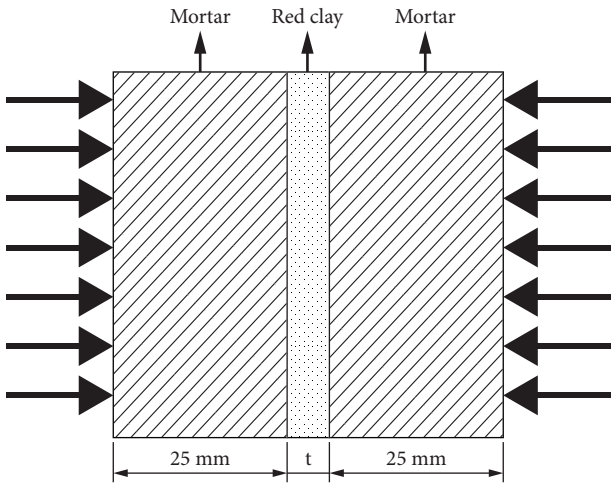

Figure 2: Schematic diagram of the composite specimen with different filling medium thicknesses.

Figure 4 shows that the effective stresses of the composite specimens with strain rates of 75.8 s^{-1}, 67.8 s^{-1}, 53.7 s^{-1}, and 43.2 s^{-1} are 24.25 MPa, 18.33 MPa, 13.79 MPa, and 10.87 MPa, respectively, and the time required to reach the peak stress is 25.4 μs, 28.7 μs, 31.0 μs, and 32.1 μs, respectively. With increasing loading pressure, the effective stress of the specimen increases, but the time required to reach the peak stress decreases because the energy carried by the stress wave (incident energy) gradually increases with increasing loading air pressure and the moisture content and thickness of the filling medium remain unchanged at this time. Therefore, the blocking effect of the filling medium on the stress wave is the same. The energy consumed by the filling medium is the same, and the strength of the transmitted stress wave increases with increasing impact air pressure, which shortens the propagation time of the stress wave.

The different thicknesses and water contents of the filling medium have a direct impact on the propagation of the stress wave in the specimen. When the strain rate is 75.8 s^{-1} and the water content W is 36%, the influence of different thicknesses of the filling medium on the stress-time history curve of the specimen is shown in Figure 5.

Figure 5 shows that when the strain rate is consistent with the water content, the peak stress of the composite specimen decreases gradually with the increase of the thickness of the filling medium and the time to reach the peak stress increases gradually with the increase in the thickness d of the filling medium. Compared with the specimen with a thickness of 3 mm, the effective stress decreases of the specimens with thicknesses of 6 mm and 9 mm are 8.2% and 20.6%, respectively, and the propagation time to the peak stress increases by 4.0% and 17.6% because the wave impedance of the joint (red clay) does not match the wave impedance of the mortar on both sides. When the stress wave passes through the mortar-joint-mortar composite specimen, the stress wave will be reflected at the two interfaces of the mortar and red clay. When the thickness of the filling medium d increases, the reflection time gradually decreases and the greater the influence of the thickness of the filling medium on the propagation of the stress wave will be. The filling medium consumes a large amount of energy carried by the stress wave, and the attenuation of the stress wave energy intensifies. The peak stress of the specimen decreases with the decrease in the transmitted stress wave. The greater the thickness of the medium is, the longer the wave propagation time in the medium and the longer the time for the specimen to reach the peak stress.

Figure 6 shows the relationship between the water content and effective stress of the composite specimen when the strain rate is consistent with the filling thickness.

Figure 6 shows that when the strain rate is consistent with the filling thickness, as the water content of the filling medium increases, the lag time of stress wave propagation is longer and the effective stress of the composite decreases accordingly. Compared with the specimen with a water content of 36%, the effective stress decreases by 13.2%, 31.0%, and 54.4% when the water content is 39%, 42%, and 45%, respectively. The propagation time to peak stress increased by 8.3%, 18.4%, and 21.9% because with the increase in the water content in the filling medium, the propagation velocity V of the stress wave in the filling medium decreases gradually and the time for the stress wave to reach the peak stress increases accordingly. As the water content of the filling medium increases, the wave impedance decreases gradually, the reflected wave of the stress wave increases

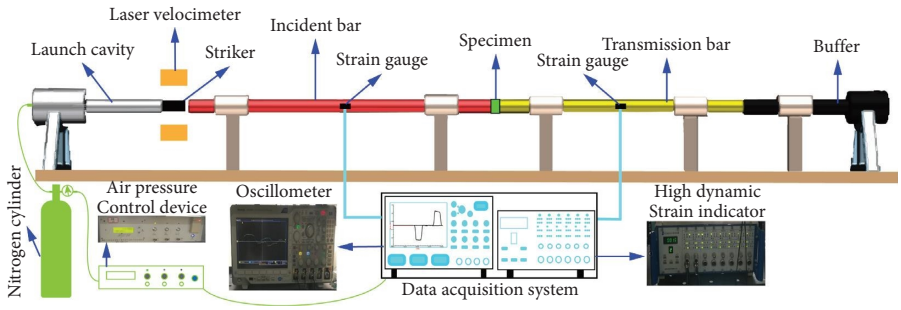

Figure 3: Schematic diagram of the SHPB test device.

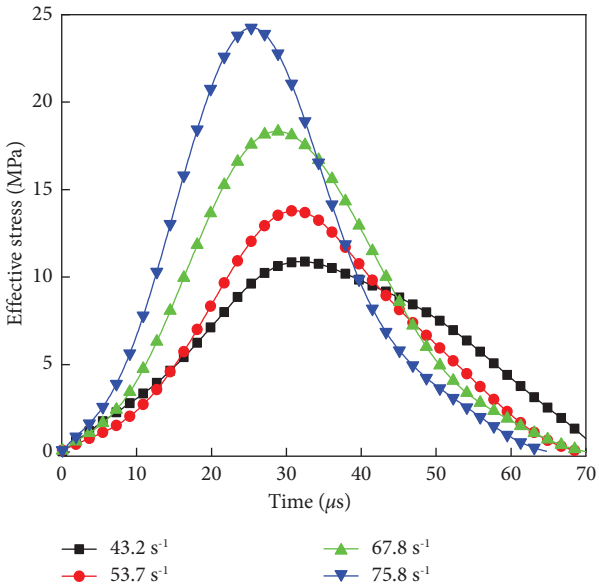

Figure 4: Effective stress-time history curve of the specimen under different strain rates when d is 3 mm and W is 42%.

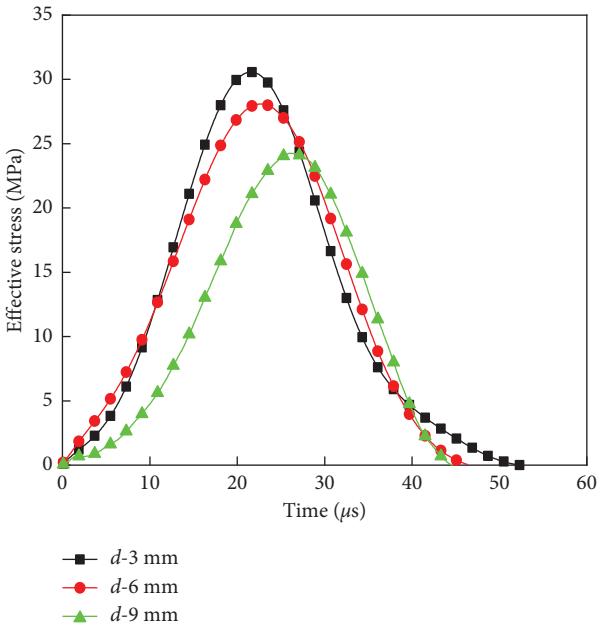

Figure 5: Stress-time history curve of composite specimens with different filling medium thicknesses.

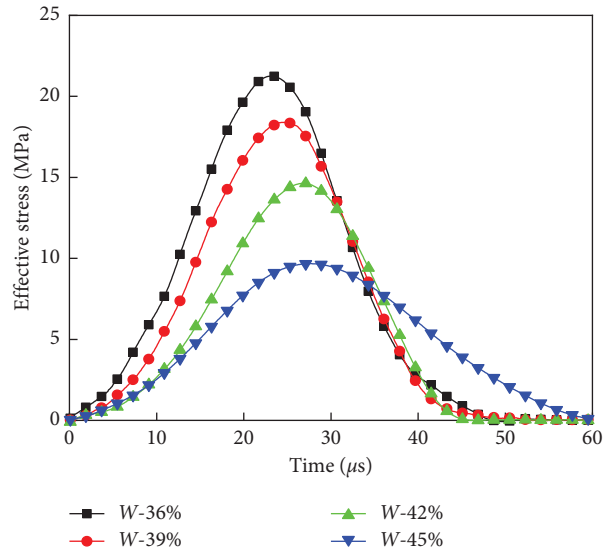

Figure 6: Stress-time history curve of composite specimens with different moisture contents when d is 6 mm.

gradually at the interface between the filling medium and mortar, the transmission wave decreases, and the peak stress decreases accordingly.

3.2. Stress-Strain Curve. Figure 7 shows the influence of the thickness and water content of the filling medium on the stress-strain curve of the composite specimen under the same impact pressure.

Figure 7 shows that under the same strain rate, as the thickness and water content of the filling medium increase, the slope of the curve of the specimen in the elastic stage decreases significantly, the elastic variation section of the specimen becomes shorter, and the corresponding initial elastic modulus decreases. The dynamic compressive strength and dynamic elastic modulus also decrease significantly with increasing thickness and water content of the filling medium, and the nonlinear deformation of the specimen is more obvious with increasing thickness and water content of the filling medium.

The decline form of the postpeak stress-strain curve represents the degree of failure of the specimen. The decline form of the mortar-joint-mortar composite specimen with

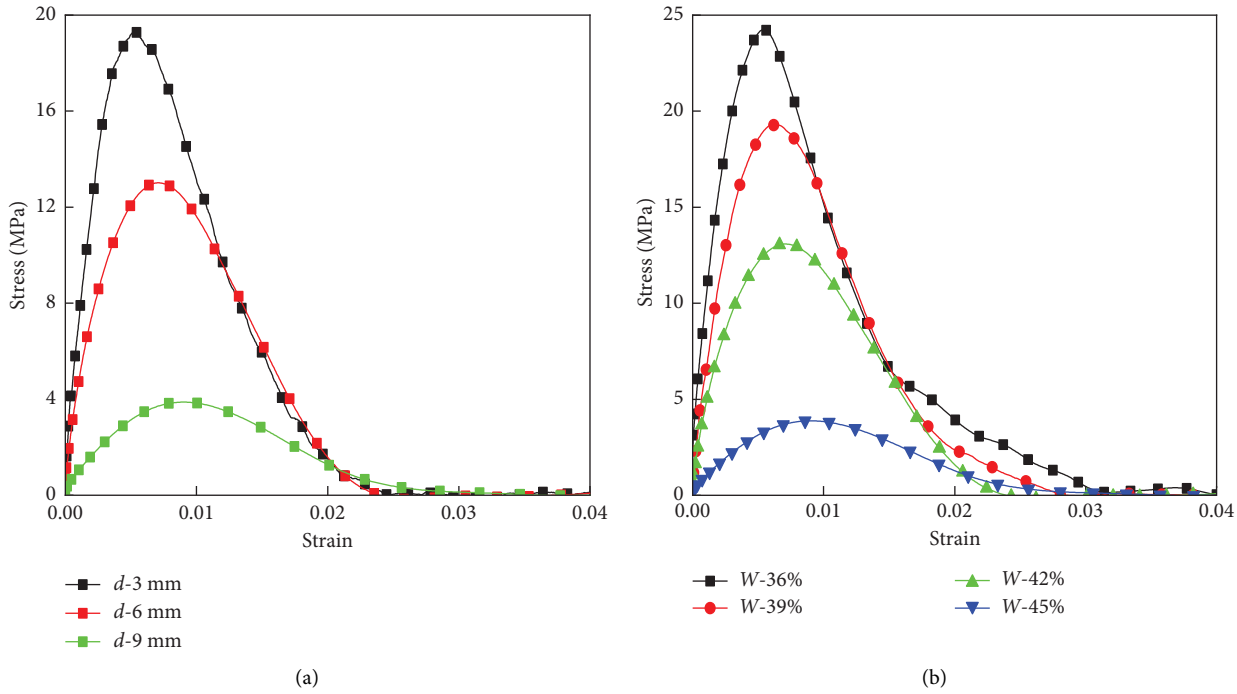

FIGURE 7: Dynamic stress-strain curve of the composite specimen. (a) *W* is the stress-strain curve of the composite specimen at 45%. (b) *d* is the stress-strain curve of the composite specimen under 9 mm.

different water contents and thicknesses of the filling medium is different after reaching the stress peak. According to the stress-strain curve, the thickness *d* and water content *W* of the filling medium increase, the slope of the postpeak curve decreases significantly, the peak strain of the specimen increases significantly, and the postpeak deformation is aggravated. The results show that the plastic deformation capacity of the specimen increases with increasing thickness *d* and water content *W* of the filling medium, mainly because the filling medium (red clay) has a strong plastic deformation ability and the increase in the thickness and water content of the filling medium enhances the plastic deformation ability of the specimen.

3.3. Relationship between Peak Stress and Strain Rate, Thickness of the Filling Medium, and Water Content. When the water content of the filling medium *W* is 36%, the fitting curve of the peak stress and strain rate of the mortar-red clay-mortar composite specimens with different filling medium thicknesses *d* is shown in Figure 8. When the filling medium thickness *d* is 3 mm, the fitting curve of the peak stress and strain rate of the mortar-red clay-mortar composite specimens with different joint water contents *W* is shown in Figure 9.

The fitting curves in Figures 8 and 9 show that the specimen of the mortar-red clay-mortar composite has an obvious strain rate effect. With an increasing strain rate, the composite peak stress increases and there is a strong power correlation. The increase in the strain rate shortens the action time of the impact load, and the specimen does not have enough time to accumulate energy. According to the functional principle, the specimen can only balance the external energy by increasing the stress, so the peak stress increases gradually with an increasing strain rate. The fitting curve relationship also shows that the thickness and water content of the filling medium also affect the rate correlation of the strength of the composite specimen, but with the increase in the thickness and water content of the filling medium, the slope of the fitting curve gradually decreases, indicating that with the increase in the thickness and water content of the filling medium, the sensitivity of the peak stress of the composite specimen to the strain rate gradually decreases.

When the strain rate is 75.8 s^{-1}, the fitting curve between the filling medium thickness and water content and the peak stress of the composite specimen is shown in Figure 10, and the fitting relationship is shown in Table 1.

Figure 10 and Table 1 show that with increasing thickness *d* and water content *W* of the filling medium, the peak stress of the mortar-joint-mortar combination specimen gradually decreases and there is a good linear negative correlation between the thickness, water content, and peak stress because when the stress wave passes through the filling medium, filling medium thickness *d,* and the increase of water content *W*, more stress wave reflection and absorption cut through the joints and the stress wave, namely, filling medium stress wave energy expenditures increase and the barrier for the filling medium of the stress wave along with the increase in the thickness and the moisture content is significantly enhanced. The stronger the weakening effect on the peak stress of the composite specimen is, the lower the peak stress is macroscopically.

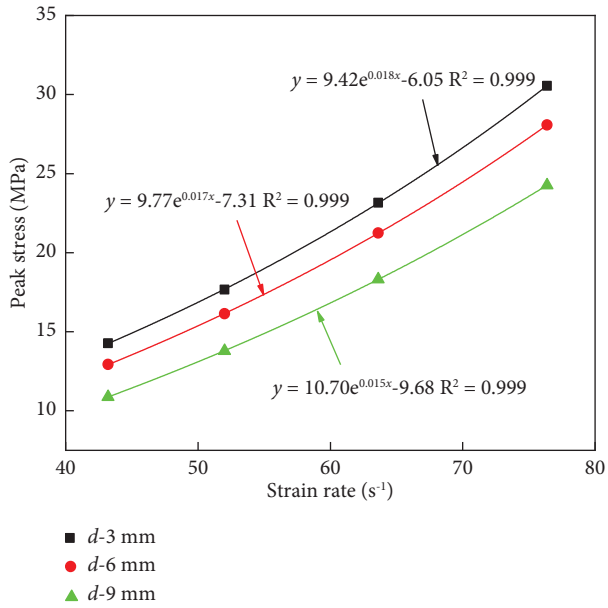

Figure 8: Relationship between the peak stress and strain rate of the composite specimen when the water content is 36%.

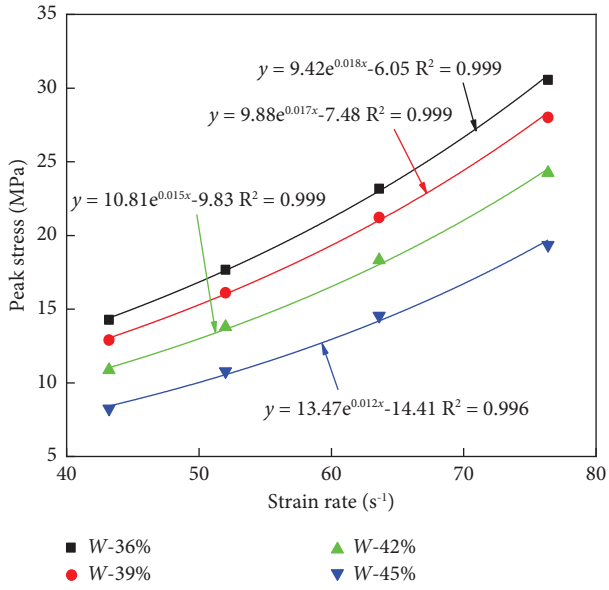

Figure 9: Relationship between the peak stress and strain rate of the composite specimen with medium thickness of 3 mm.

3.4. Variation Law of Energy Dissipation of Composite Specimens. The damage and failure process of the assembly can be regarded as the result of the mutual transformation of different forms of energy. The stress-strain state of the material at different time periods corresponds to the corresponding energy state. Energy analysis can avoid analyzing the complex deformation process, which is more conducive to the study of the failure essence of the composite specimen [42]. The energy variation law of the composite specimen under different strain rates is shown in Figure 11. When the strain rate is 75.8 s^{-1}, the influence law of the medium thickness and moisture content on the crushing energy consumption density of the composite specimen is shown in Figure 12.

According to Figure 11, with increasing strain rate, each energy increases continuously. Under different strain rates, the incident energy > the reflection energy > the dissipation energy > the transmission energy. From the slope of the curve, the transmission energy increases relatively gently with increasing strain rate. The analysis shows that due to the large difference in wave impedance between the mortar specimen and compression bar and between the red clay and mortar specimen, when the incident wave acts on the incident bar and the front mortar end face, due to the poor matching of wave impedance between the mortar and incident bar, more energy is reflected back to the incident bar to form reflected energy and a small part of the energy passes through the front mortar specimen into red clay. At this time, due to the large difference in wave impedance between the red clay and the rear mortar specimen, more energy is reflected and a small part of the energy passes through the red clay and is transmitted to the rear mortar specimen. Similarly, due to the large difference between the wave impedance of the rear mortar specimen and the transmission rod, only a small part of the energy is transferred to the transmission rod to form the transmission energy. At the same time, with the increase in joint thickness and water content, the joint consumes more energy from the stress wave, the energy attenuation of the stress wave intensifies, and the transmission energy is smaller.

Figure 12 shows that the thickness and moisture content of the backfill medium have an impact on the crushing energy density of the composite specimen. When the thickness of the medium is the same, the crushing energy density of the specimen increases significantly with increase in moisture content of the medium. When the thickness of the medium is 3 mm, compared with the sample with 36% moisture content, when the water content was 39%, 42%, and 45%, the crushing energy consumption decreased by 2.13%, 6.53%, and 11.06%, respectively, and the decrease gradually increased. Under the same water content, with the increase in filling medium thickness, the energy dissipation density of the specimen also decreases and the increase in filling medium thickness and water content will reduce the energy dissipation density of the composite specimen.

3.5. Failure Mode of the Composite Specimen. Figure 13 shows the failure morphology of the mortar-red clay-mortar composite specimens with different water contents and different filling medium thicknesses (d) in the filling medium at a strain rate of 75.8 s^{-1}.

Figure 13 shows the same filling medium thickness, moisture content, and strain rate; contact with the broken incident bar mortar test block was significantly higher than contact with the transmission rod mortar test block because the joint surface occurred in the stress wave propagation attenuation, the joint surface energy was received by its back-end mortar test block below the front specimen, and the degree of specimen breakage was reduced. The change in the filling medium thickness will lead to the difference in the

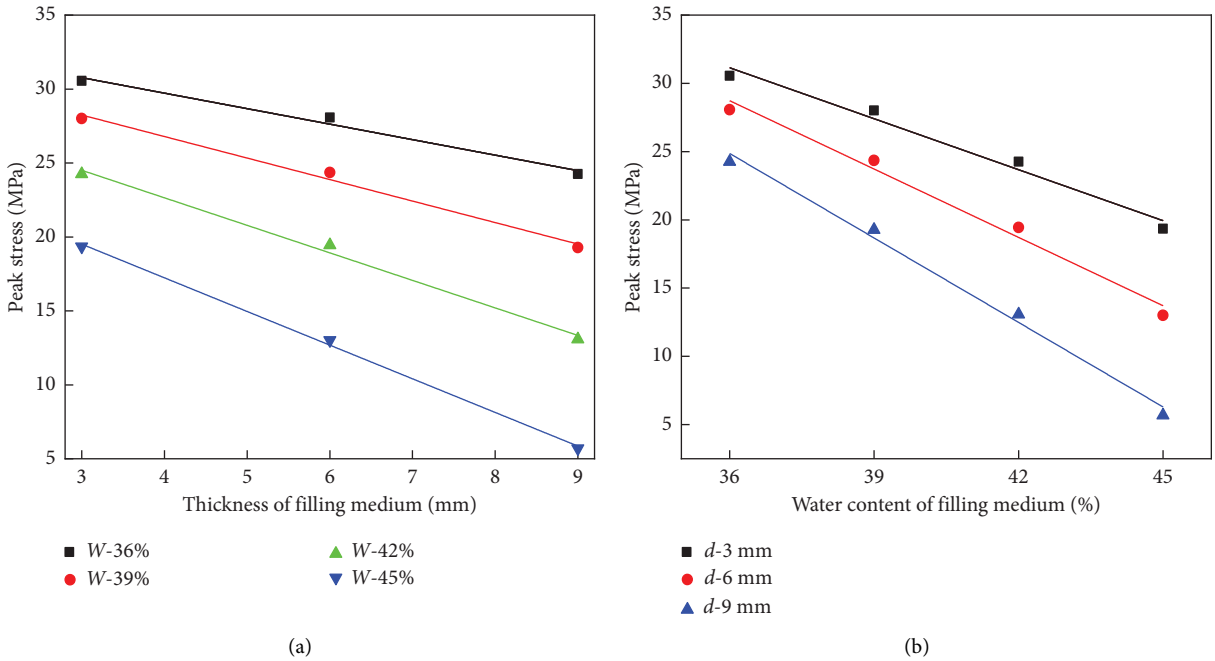

Figure 10: Variation in the dynamic compressive strength of the composite specimen. (a) Relationship between peak stress and filling medium thickness. (b) Relationship between the peak stress and water content of the filling medium.

Table 1: Peak stress fitting curve.

Filling thickness d (mm) and water cut W	Fitting formula	R^2
W-36%	$\sigma = -1.05d + 33.92$	0.970
W-39%	$\sigma = -1.46d + 32.61$	0.982
W-42%	$\sigma = -1.86d + 30.09$	0.987
W-45%	$\sigma = -2.28d + 26.34$	0.996
d-3	$\sigma = -1.25W + 38.72$	0.971
d-6	$\sigma = -1.67W + 38.72$	0.978
d-9	$\sigma = -2.06W + 38.72$	0.989

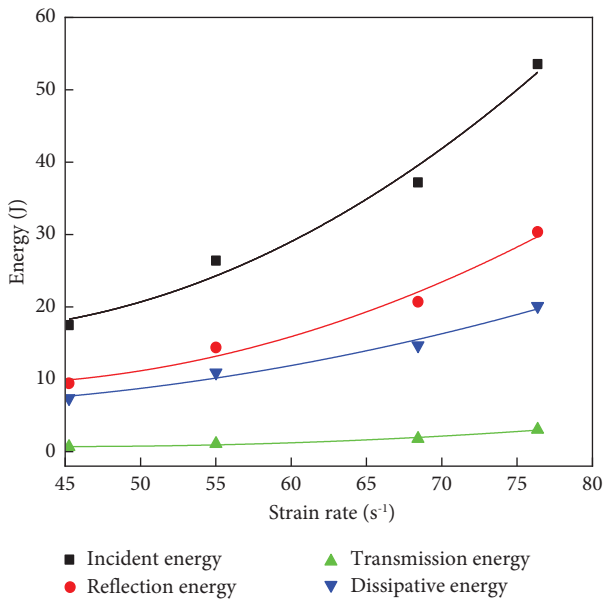

Figure 11: Stress-time history curve of composite specimens with different filling medium thicknesses.

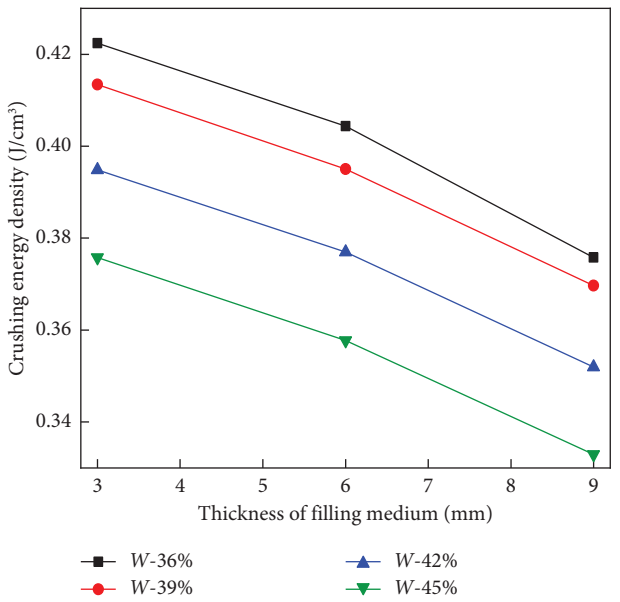

Figure 12: Variation law of crushing energy consumption density of composite specimens.

degree of fracture and fragment size of the mortar specimen on both sides of the joint. Under the same loading pressure, with the increase of d, there is no significant difference in the degree of breakage of the mortar specimen at the incident rod end, while the degree of breakage of the mortar specimen at the transmission rod end decreases significantly. This is because when the impact pressure remains unchanged, the energy absorbed by the specimen at the incident rod end is similar, and the damage degree does not change much. With the increase in d, the energy absorbed by

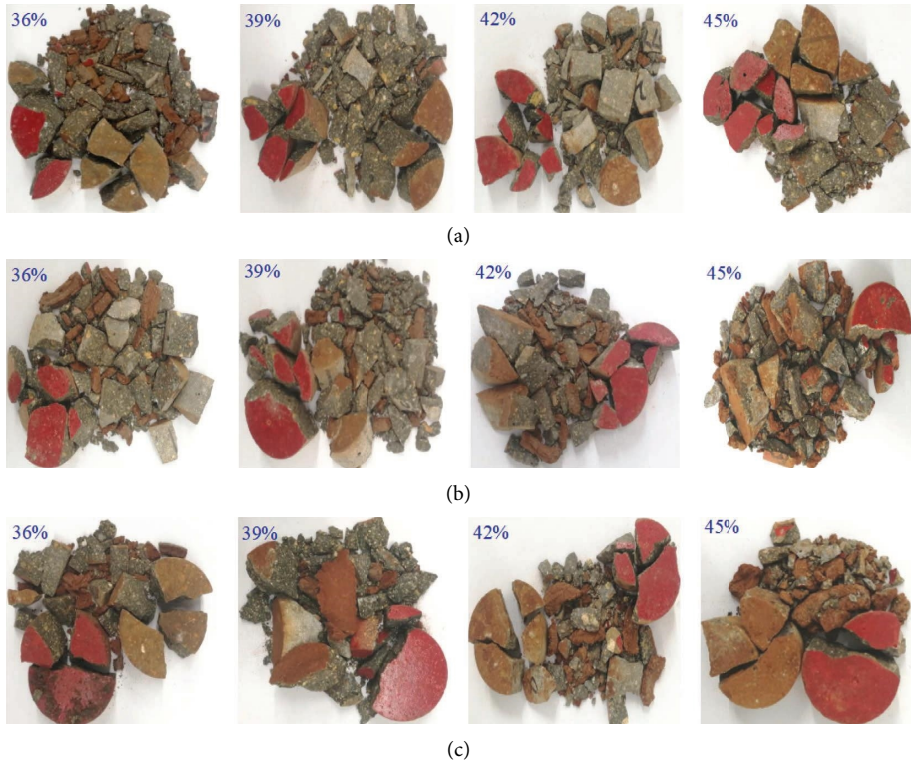

FIGURE 13: Failure modes of composite specimens with different filling media thicknesses and water contents. (a) $d = 3$ mm. (b) $d = 6$ mm. (c) $d = 9$ mm.

the filling body increases, while the energy that reaches the rear mortar specimen through the filling joint surface is less. When the stress wave spreads to the rear mortar, the energy value received by the specimen decreases, so the degree of damage to the rear mortar decreases gradually with an increasing d.

The water content of the filling medium also affects the failure mode of the composite specimen. When d and strain rate are the same, the change of water content W makes the damage degree of the specimen different. The damage degree of the transmission rod end specimen decreases with the increase of W. Joint plane wave impedance decreases, with the increase of W in the mortar-joint surface reflecting wave increases and the joints and absorbed energy gradually increase. The attenuation of stress wave energy through the joint plane to the specimen at the back end is intensified, the energy absorbed by the mortar specimen at the back end of the joint plane is reduced, and the degree of failure of the specimen is reduced.

4. Conclusions

(1) When the strain rate was 75.8 s^{-1}, 67.8 s^{-1}, 53.7 s^{-1}, and 43.2 s^{-1}, the effective stresses of the specimens were 24.25 MPa, 18.33 MPa, 13.79 MPa, and 10.87 MPa, respectively. The time required to reach the peak stress was 25.4 μs, 28.7 μs, 31.0 μs, and 32.1 μs, respectively. With increasing strain rate, the peak value of the stress wave increases and the time to reach the peak stress decreases.

(2) When the strain rate is 75.8 s^{-1} and the water content W is 36%, compared with the specimens with a thickness of 3 mm, the peak stress of the specimens with thicknesses of 6 mm and 9 mm decreases by 8.2% and 20.6%, respectively, and the propagation time to reach the peak stress increases by 4.0% and 17.6%. When d is 6 mm, compared with the specimen with 36% moisture content, the peak stress decreases by 13.2%, 31.0%, and 54.4% at 39%, 42%, and 45% moisture content, respectively, and the propagation time to peak stress increases by 8.3%, 18.4%, and 21.9%. With the increase in the thickness and water content of the filling medium, the peak stress of the specimen gradually decreases and the time to reach the peak stress gradually increases.

(3) The peak stress and energy of the specimens increased with an increasing strain rate. When the strain rate is 75.8 s^{-1} and the thickness of the medium is 3 mm, compared with the samples with 36% water content, the breakage energy consumption decreases by 2.13%, 6.53%, and 11.06% at 39%, 42%, and 45% water content. The increase in thickness d and moisture content W of the filling medium reduces the peak stress and energy dissipation density of crushing, and there is a linear negative correlation between peak stress and thickness d and moisture content W of the filling medium.

(4) Under the same filling medium thickness, water content, and strain rate, the degree of failure of the mortar specimen at the incident rod end is higher

than the degree of failure of the mortar specimen at the transmitted rod end and the existence of a joint plane causes stress wave attenuation during the propagation process. With the increase in the filling medium thickness d and water content W, the stress wave energy attenuation is aggravated and the degree of fracture of the test block at the back of the joint surface is reduced.

Data Availability

The data presented in this study are available on request from the corresponding author.

Conflicts of Interest

The authors declare that they have no conflicts of interest.

Acknowledgments

This work was supported by the Science and Technology Foundation of Guizhou Provincial Transportation Department (nos. 2017-123-010 and 2016-121-032).

References

[1] M. F. Cai, *Rock Mechanics and Engineering*, Science Press, Beijing, China, 2013.

[2] Z. C. Xia and Z. Q. Sun, *Joint Mechanics of Engineering Rock Mass*, Tongji University Press, Shanghai, China, 2002.

[3] B. Indraratna, M. Jayanathan, and E. T. Brown, "Shear strength model for overconsolidated clay-infilled idealised rock joints," *Géotechnique*, vol. 58, no. 1, pp. 55–65, 2008.

[4] B. Indraratna, D. A. F. Oliveira, E. T. Brown, and A. P. de Assis, "Effect of soil-infilled joints on the stability of rock wedges formed in a tunnel roof," *International Journal of Rock Mechanics and Mining Sciences*, vol. 47, no. 5, pp. 739–751, 2010.

[5] H. B. Li, H. J. Jiang, and J. Zhao, "Several safety problems of rock mass engineering under dynamic load," *Chinese Journal of Rock Mechanics and Engineering*, vol. 22, no. 11, pp. 1887–1891, 2003.

[6] Z. Zhou, L. Zhang, and H. J. Hou, "Study on the influence of filling on mechanical properties and energy evolution of jointed rock mass," *Water Resources and Hydropower Technology*, vol. 51, no. 7, pp. 117–123, 2020.

[7] S. B. Chai, H. Wang, Y. L. Jing, and N. Jia, "Experimental study on dynamic compression characteristics of rock filled with joint accumulated damage," *Journal of Rock Mechanics and Engineering*, vol. 39, no. 10, pp. 2025–2037, 2020.

[8] L. Lian, S. B. Zhang, Y. Wang, G. Wang, and H. Wang, "Study on macro and micro mechanism of shear failure of joint surfaces with different filling thicknesses," *Journal of Guangxi University (Natural Science Edition)*, vol. 44, no. 3, pp. 756–764, 2019.

[9] G. K. Zhang, H. B. Li, X. Xia, N. N. Li, and S. B. Chai, "The influence of joint characteristics on the mechanical properties of rock mass," *Journal of Central South University*, vol. 47, no. 12, pp. 4198–4205, 2016.

[10] C. L. Ao, "Effect of weak interlayer on stress wave propagation in explosion," *Blasting*, vol. 5, no. 2, pp. 23–27, 1988.

[11] L. J. Pyrak-nolte, "The seismic response of fractures and the interrelation among fracture properties," *International Journal of Rock Mechanics and Mining Sciences*, vol. 33, no. 8, pp. 787–802, 1996.

[12] J. G. Cai and J. Zhao, "Effects of multiple parallel fractures on apparent attenuation of stress waves in rock masses," *International Journal of Rock Mechanics and Mining Sciences*, vol. 37, no. 4, pp. 661–682, 2000.

[13] M. Y. Wang and Q. H. Qian, "Attenuation law of explosion stress wave through joint fissure zone," *Chinese Journal of Geotechnical Engineering*, vol. 14, no. 2, pp. 42–46, 1995.

[14] W. W. Guo, S. R. Wang, and S. F. Chen, "Effect of joints in rock mass on blasting action," *Explosion and Shock Waves*, vol. 19, no. 2, pp. 93–97, 1999.

[15] S. L. Jia, Z. L. Wang, F. Xiong, N. C. Tian, and Z. T. Lu, "Study on propagation characteristics of stress waves in rock mass filled with joints," *Journal of Hefei University of Technology*, vol. 44, no. 8, pp. 1073–1081, 2021.

[16] Y. X. Ding, Z. L. Wang, and Y. P. Huang, "Three dimensional simulation of stress wave propagation in jointed rock mass with filling," *Journal of Water Resources and Water Transport Engineering*, vol. 6, pp. 80–88, 2020.

[17] T. T. Liu, X. P. Li, H. B. Li, J. C. Li, and Y. Luo, "Numerical study on the propagation law of stress waves in rock mass filled with joints," *Journal of Rock Mechanics and Engineering*, vol. 32, no. S2, pp. 3552–3560, 2016.

[18] X. F. Chen, X. X. Zhao, H. B. Wang, L. Ma, and C. B. Wang, "Model test and application study on the propagation law of explosion stress wave in jointed filled rock mass," *Science and Technology of Work Safety in China*, vol. 14, no. 12, pp. 130–134, 2018.

[19] P. Shao, Y. Zhang, Y. N. He, and T. Jiang, "Experimental study on fatigue failure of intermittently jointed rock mass under repeated stress waves," *Chinese Journal of Rock Mechanics and Engineering*, vol. 22, pp. 4180–4184, 2005.

[20] N. C. Xu, M. J. Zhao, and D. L. Wu, "Research on stress wave inversion model of jointed rock mass," *Rock and Soil Mechanics*, vol. 12, pp. 2705–2710, 2007.

[21] J. Dong, L. Ding, L. Wang et al., *Blasting*, vol. 45, no. 1, pp. 17–25, 2021.

[22] Z. D. Deng, H. Y. Liu, and X. S. Wang, "Hopkinson experimental study on strength and failure characteristics of jointed rock mass under dynamic load," *Mining Research and Development*, vol. 34, no. 1, pp. 68–72, 2014.

[23] Q. Y. Ma, Q. Q. Su, D. D. Ma, and P. Yuan, "Experimental study on SHPB dynamic mechanical failure characteristics of deep roadway sandstone with different joint dip angles," *Journal of Rock Mechanics and Engineering*, vol. 39, no. 6, pp. 1104–1116, 2020.

[24] Y. Tsubota, Y. Iwakoke, and R. Yoshinaka, "Dynamic mechanical properties of rock joints under cyclic loading using ryoke gneiss," in *Proceedings of the 2014 ISRM International Symposium—8th Asian RockMechanics Symposium*, pp. 741–748, Sapporo, Japan, October 2014.

[25] S. M. M. Niktabar, K. S. Rao, and A. K. Shrivastava, "Effect of rock joint roughness on its cyclic shear behavior," *Journal of Rock Mechanics and Geotechnical Engineering*, vol. 9, no. 6, pp. 1071–1084, 2017.

[26] G. Walton, L. R. Alejano, J. Arzua, and T. Markley, "Crack damage parameters and dilatancy of artificially jointed granite samples under triaxial compression," *Rock Mechanics and Rock Engineering*, vol. 51, no. 6, pp. 1637–1656, 2018.

[27] J. B. Zhu, X. B. Zhao, W. Wu, and J. Zhao, "Wave propagation across rock joints filled with viscoelastic medium using modified recursive method," *Journal of Applied Geophysics*, vol. 86, pp. 82–87, 2012.

[28] S. B. Chai, J. C. Li, Q. B. Zhang, H. B. Li, and N. N. Li, "Stress wave propagation across a rock mass with two non-parallel joints," *Rock Mechanics and Rock Engineering*, vol. 49, no. 10, pp. 4023–4032, 2016.

[29] J. C. Li, N. N. Li, H. B. Li, and J. Zhao, "An SHPB test study on wave propagation across rock masses with different contact area ratios of joint," *International Journal of Impact Engineering*, vol. 105, pp. 109–116, 2017.

[30] J. C. Li and G. W. Ma, "Analysis of blast wave interaction with a rock joint," *Rock Mechanics and Rock Engineering*, vol. 43, no. 6, pp. 777–787, 2010.

[31] J. C. Li, L. F. Rong, H. B. Li, and S. N. Hong, "An SHPB test study on stress wave energy attenuation in jointed rock masses," *Rock Mechanics and Rock Engineering*, vol. 52, no. 2, pp. 403–420, 2019.

[32] D. X. Lei, H. Lin, and Y. X. Wang, "Damage characteristics of shear strength of joints under freeze–thaw cycles," *Archive of Applied Mechanics*, vol. 92, no. 5, pp. 1615–1631, 2022.

[33] H. Lin, D. X. Lei, R. Yong, C. Jiang, and S. G. Du, "Analytical and numerical analysis for frost heaving stress distribution within rock joints under freezing and thawing cycles," *Environmental Earth Sciences*, vol. 79, no. 12, p. 305, 2020.

[34] J. C. Bian, *Numerical simulation study on propagation law of explosion stress wave in jointed rock mass*, Xi'an University of Architecture and Technology, Xi'an, China, 2018.

[35] T. T. Liu, X. P. Li, and H. B. Li, "Numerical study of stress wave propagation in filling jointed rock mass," *Chinese Journal of Rock Mechanics and Engineering*, vol. 35, no. S2, pp. 3552–3560, 2016.

[36] X. B. Zhao, J. Zhao, J. G. Cai, and A. Hefny, "UDEC modelling on Wave propagation across fractured rock masses," *Computers and Geotechnics*, vol. 35, no. 1, pp. 97–104, 2008.

[37] F. W. Yang, H. B. Li, and J. C. Li, "Numerical simulation of stress wave propagation characteristics of oblique entry ray elastic joints," *Rock and Soil Mechanics*, vol. 35, no. 3, pp. 901–907, 2013.

[38] H. F. Deng, J. L. Li, C. J. Deng, L. H. Wang, and T. Lu, "Study on sample selection and compressive strength prediction method in rock mechanics test," *Geotechnical mechanics*, vol. 32, no. 11, pp. 3399–3403, 2011.

[39] H. B. Wang, G. L. Zhai, M. X. Wang, and Q. Zong, "Study on test and analysis method of dynamic mechanical properties of coal mine sandstone," *China work safety science and technology*, vol. 17, no. 5, pp. 53–59, 2021.

[40] L. Song and S. S. Hu, "Two wave method and three wave method in SHPB data processing," *Shock and explosion*, vol. 25, no. 4, pp. 368–373, 2005.

[41] W. Tian, C. Yu, X. H. Wang, and P. F. Wu, "Study on dynamic mechanical properties and energy dissipation of 3D printed fractured rock mass," *Chinese Journal of Rock Mechanics and Engineering*, vol. 41, no. 3, pp. 446–456, 2022.

[42] R. R. Zhang and L. W. Jing, "Analysis on the relationship between deep sandstone fragmentation degree and energy dissipation after high and low temperature in SHPB test," *Journal of coal*, vol. 43, no. 7, pp. 1884–1892, 2018.